Chinese Journal of Natural Medicines

Ent–pimarane and *ent*–kaurane diterpenoids from *Siegesbeckia pubescens* and their anti–endothelial damage effect in diabetic retinopathy

Mengjia Liu, Tingting Luo, Rongxian Li, Wenying Yin, Fengying Yang, Di Ge, Na Liu

Citation: Mengjia Liu, Tingting Luo, Rongxian Li, Wenying Yin, Fengying Yang, Di Ge, Na Liu, *Ent*–pimarane and *ent*–kaurane diterpenoids from *Siegesbeckia pubescens* and their anti–endothelial damage effect in diabetic retinopathy, Chinese Journal of Natural Medicines, 2025, 23(2), 234–244. doi: 10.1016/S1875–5364(25)60827–2.

View online: https://doi.org/10.1016/S1875–5364(25)60827–2

Chinese Journal of Natural Medicines 23 (2025) 234-244

Contents lists available at ScienceDirect

Chinese Journal of Natural Medicines

journal homepage: www.cjnmcpu.com/

Original article

Ent-pimarane and *ent*-kaurane diterpenoids from *Siegesbeckia pubescens* and their anti-endothelial damage effect in diabetic retinopathy

Mengjia Liu[Δ], Tingting Luo[Δ], Rongxian Li, Wenying Yin, Fengying Yang, Di Ge[*], Na Liu[*]

School of Biological Science and Technology, University of Jinan, Jinan 250022, China

ARTICLE INFO

Article history:
Received 16 March 2024
Revised 28 April 2024
Accepted 17 June 2024
Available online 20 February 2025

Keywords:
Siegesbeckia pubescens
Natural diterpenoid
Diabetic retinopathy
Oxidative stress
Inflammatory response

ABSTRACT

Diabetic retinopathy, a prevalent and vision-threatening microvascular complication of diabetes mellitus, is the leading cause of blindness among middle-aged and elderly individuals. Natural diterpenoids isolated from *Siegesbeckia pubescens* demonstrate potent anti-inflammatory properties. This study aimed to identify novel bioactive diterpenoids from *S. pubescens* and investigate their effects on oxidative stress and inflammatory responses in diabetic retinopathy, both *in vitro* and *in vivo*. Three new *ent*-pimarane-type diterpenoids (**1**–**3**) and six known compounds (**4**–**9**) were isolated from the aerial parts of *S. pubescens*. Their structures were elucidated through spectroscopic data interpretation, and absolute configurations were determined by comparing calculated and experimental electronic circular dichroism (ECD) spectra. Among these compounds, 14*β*,16-epoxy-*ent*-3*β*,15*α*,19-trihydroxypimar-7-ene (**5**) exhibited the most potent protective effect against high glucose and interleukin-1β (IL-1β)-stimulated human retinal endothelial cells. Mechanistically, compound **5** promoted endothelial cell survival while ameliorating oxidative stress and inflammatory response in diabetic retinopathy, both *in vivo* and *in vitro*. These findings not only suggest that diterpenoids such as compound **5** are important anti-inflammatory constituents in *S. pubescens*, but also indicate that compound **5** may serve as a lead compound for preventing or treating vascular complications associated with diabetic retinopathy.

1. Introduction

Diabetic retinopathy (DR), a microvascular complication of diabetes induced by hyperglycemia, leads to various pathophysiological alterations, including endothelial dysfunction, inflammation, and oxidative stress. It is the primary cause of preventable blindness among working-age individuals [1, 2]. The incidence of DR is projected to increase from 424.9 million in 2017 to approximately 628 million by 2045, substantially elevating the challenges associated with effective disease management [3]. Current therapeutic options for DR, such as corticosteroids or targeted treatments against vascular endothelial growth factor (VEGF), are limited by short circulating half-lives and necessitate frequent intraocular administration [4, 5]. Consequently, there is an urgent need to identify novel, efficacious pharmaceutical interventions for DR treatment.

Natural products with exceptional safety and efficacy play an increasingly significant role in drug discovery research, with some demonstrating potential for treating DR [6]. *Siegesbeckia pubescens* Makino, a primary plant source of Siegesbeckiae Herba, is widely distributed across China. Traditionally, its aerial parts have been utilized in Chinese medicine to treat hypertension, stroke, and various inflammatory diseases, including gout and rheumatoid arthritis [7]. Phytochemical investigations of this medicinal plant have revealed *ent*-pimarane and *ent*-kaurane diterpenoids as their principal constituents, exhibiting significant anti-inflammatory activity [8]. For instance, kirenol, a major *ent*-pimarane diterpenoid isolated from Herba Siegesbeckia, inhibits nuclear factor kappa B (NF-*κ*B) signaling activation and pro-inflammatory cytokine expression, demonstrating anti-inflammatory responses in collagen-induced arthritis. Notably, kirenol has shown anti-inflammatory effects in a rat model of diabetic inflammation, as evidenced by pharmacological studies [9-11]. Although *S. pubescens* is recognized for its significant benefits, its biological potential for mitigating oxidative stress and inflammatory responses in DR remains unexplored. Therefore, this study aimed to identify new bioactive diterpenoids from *S. pubescens* and investigate their effects on oxidative stress and inflammatory responses both *in vivo* and *in vitro* in DR. Three novel *ent*-pimarane-type diterpenoids (**1**–**3**) along with six known compounds (**4**–**9**) were isolated from the aerial parts of *S. pubescens*. Their structures were elucidated through spectroscopic data interpretation, and absolute configurations were determined by comparing calculated and experimental electronic circular dichroism (ECD) spectra. Among these compounds, 14*β*,16-epoxy-*ent*-3*β*,15*α*,19-trihydroxypimar-7-ene (**5**) demonstrated the most potent protective effect against high glucose and interleukin-1 beta (IL-1β)-stimulated human retinal endothelial cells (HRECs). Mechanistic-

* Corresponding author.
E-mail addresses: bio_ged@ujn.edu.cn (D. Ge); mls_liun@ujn.edu.cn (N. Liu)
Δ These authors contributed equally to this work.

https://doi.org/10.1016/S1875-5364(25)60827-2

ally, this study revealed that compound **5** promoted endothelial cell survival and ameliorated oxidative stress and inflammatory responses both *in vivo* and *in vitro* in DR. These findings not only suggest that diterpenoids such as compound **5** are important anti-inflammatory constituents in *S. pubescens*, but also indicate that compound **5** may serve as a lead compound for the prevention and treatment of vascular complications in DR. This study may provide valuable insights for future pharmaceutical approaches to treating DR.

2. Results

2.1. Structure determination of new and known diterpenoids

Compound **1** was isolated as a white, amorphous powder. Its molecular formula was determined to be $C_{18}H_{24}O_2$ based on the high-resolution electrospray ionization mass spectrometry (HR-ESI-MS) ion at *m/z* 273.1841 $[M + H]^+$ (Calcd. 273.1849), indicating seven indices of hydrogen deficiency. The infrared radiation (IR) spectrum exhibited an absorption band at ν_{max} 3435 cm^{-1}, consistent with the presence of a hydroxy group. The ^1H nuclear magnetic resonance (NMR) spectrum revealed three aromatic protons at δ_H 7.82 (1H, d, J = 1.2 Hz), 7.35 (1H, dd, J = 8.1, 1.2 Hz), and 7.24 (1H, d, J = 8.1 Hz), one oxygenated methine at δ_H 3.35 (1H, d, J = 11.4 Hz), and four tertiary methyls at δ_H 2.35 (3H, s), 1.24 (3H, s), 1.06 (3H, s) and 0.97 (3H, s). Analysis of the carbon resonances at δ_C 152.7, 136.2, 135.2, 130.5, 127.6, and 124.0 in the ^{13}C NMR spectrum, combined with the three aromatic protons in the ^1H NMR spectrum (Table 1), suggested the presence of a 1,2,4-trisubstituted aromatic ring. In addition to the signals of the trisubstituted benzene ring, the ^{13}C NMR spectrum displayed signals attributable to one ketonic carbonyl group (δ_C 199.6), four methyl groups (δ_C 27.7, 23.6, 20.9, and 15.1), three methylenes, two methines (one oxygenated at δ_C 78.3), and two aliphatic non-protonated carbons, as confirmed by the heteronuclear single quantum coherence (HSQC) spectrum. The ^1H–^1H correlation spectroscopy (COSY) spectrum revealed two discrete spin systems, H_2-1/H_2-2/H-3 and H-5/H_2-6 (Fig. 1B). The following HMBC correlations indicated the presence of a nor-pimarane diterpenoid with a hydroxy group at C-3 (Fig. 1B): from Me-17 (s, δ_H 2.35) to C-12 (δ_C 135.2), C-13 (δ_C 136.2), and C-14 (δ_C 127.6), from H-11 (δ_H 7.24) to C-8 (δ_C 130.5), C-9 (δ_C 152.7), and C-13, from Me-20 (s, δ_H 1.24) to C-1 (δ_C 36.3), C-5 (δ_C 48.7), C-9, and C-10 (δ_C 37.7), and from Me-18 (s, δ_H 1.06) and Me-19 (s, δ_H 0.97) to C-3 (δ_C 78.3), C-4 (δ_C 39.0), and C-5. Furthermore, HMBC correlations from H-5 (δ_H 1.85), H_2-6 (δ_H 2.72), and H-14 (δ_H 7.82) to the carbonyl group at δ_C 199.6 led to the assignment of a carbonyl group at position C-7. Thus, the planar structure of **1** was determined as shown in Fig. 1A. The nuclear Overhauser effect spectroscopy (NOESY) correlations from Me-20 to H-1α (δ_H 2.38) and Me-19 suggested these protons to be α-oriented, while NOESY cross-peaks from H-3 (δ_H 3.35) to H-1β (δ_H 1.69) and H-5, together with the absence of a correlation from Me-20 to H-5 led to the determination of the β-orientation of H-3 and H-5 as depicted in Fig. 1C. The absolute configuration of **1** was ultimately determined using a computational approach of quantum chemistry employing the time-dependent density functional theory (TD-DFT) method. The conformations of the isomers of **1** were generated by the isotope-resolved methane turnover dynamics gas chromatography (iMTD-GC) method embedded in the Crest program [12]. Density functional theory calculations were performed using the Gaussian 09 package. ECD spectra were calculated using the TDDFT methodology at the B3LYP/def2TZVP level utilizing integral equation formalism polarizable continuum model (IEFPCM) in methanol. The final ECD spectra were simulated by averaging the spectra of lowest energy conformers according to the Boltzmann distribution theory and their relative Gibbs free energy (ΔG). The calculated ECD spectrum for the 3*R*, 5*S*, 10*R* stereoisomer of **1** closely matched the experimental ECD spectrum (Supplementary Fig. 10). The absolute configuration of **1** was thus established as 3*R*, 5*S* and 10*R*. Consequently, compound **1** was unambiguously elucidated as 3β-hydroxy-15-devinyl-*ent*-pimar-8,11,13-triene-7-one.

Compound **2**, a white amorphous powder, exhibited a molecular formula of $C_{24}H_{36}O_6$ as evidenced by its HR-ESI-MS ion peak at *m/z* 443.2401 $[M + Na]^+$ (Calcd. for $C_{24}H_{36}O_6Na$, 443.2404). The ^1H and ^{13}C NMR spectra of **2** (Table 1) closely resembled those of **1**, with notable differences including the presence of an additional glucopyranosyl moiety and a shift in the chemical signal at the C-3 position [δ_C 84.7 (Δ +6.4)]. Furthermore, the characteristic proton signal of an anomeric doublet at δ_H 4.93 (H-1, d, J = 7.9 Hz) and complex signals at δ_H 3.96–4.58, along with six distinctive oxygenated carbons at δ_C 102.5 (C-1′), 75.2 (C-2′), 78.7 (C-3′), 72.0 (C-4′), 78.3 (C-5′), and 63.2 (C-6′) confirmed the glucopyranosyl moiety's presence. The coupling constant (J = 7.9 Hz) of the anomeric proton indicated the β-configuration of the glucopyranosyl moiety. Given that naturally occurring glucopyranosides isolated from *Siegesbeckia* species are typically in D-form and limited by the small amount of **2**, the glucopyranosyl group in **2** was tentatively assigned as D-form [13]. Key HMBC correlations from H-1′ to C-3 (δ_C 84.7) and H-3 (δ_H 3.57, dd, J = 12.0, 4.2) to C-1′ established the β-D-glucopyranosyl moiety's position at C-3 of the aglycone. A NOESY experiment revealed that the relative configuration of **2** resembled that of **1**. Consequently, the structure of **2** was elucidated as depicted.

Compound **3**, obtained as an amorphous powder, exhibited a molecular formula of $C_{20}H_{30}O_3$ as determined by HR-ESI-MS ion at *m/z* 319.2258 $[M + H]^+$. The ^1H and ^{13}C NMR spectroscopic data (Table 1) of **3** closely resembled those of **4**, with the notable exception of a keto carbonyl resonance (δ_C 217.5) in **3** replacing the oxymethine group (δ_H 3.23, δ_C 78.8) at C-3 in **4** [14]. This assignment was further corroborated by HMBC correlations from H-1 (δ_H 2.03, 1.60), Me-19 (δ_H 1.12), and H-5 (δ_H 1.67) to C-3 (δ_C 217.5). NOESY correlations from H-14 (δ_H 3.61) to Me-17 (δ_H 1.12) and H-7β (δ_H 1.99), and from H-5 to H-1β (δ_H 1.60), H-7β, and Me-18 (δ_H 1.08) suggested that Me-17, H-14, and H-5 were positioned on the same side of the molecule assigned a β-orientation. The α-orientation of Me-20 (δ_H 0.97) was inferred from NOESY correlations of Me-20/H-1α and Me-20/Me-19. The NOESY correlation between H-12 (δ_H 1.35) and H-15 (δ_H 3.89) revealed the β-orientation of OH-15 [15]. Additionally, the absence of correlations between Me-17/H-15 and H-14/H-15 further confirmed the β configuration of OH-15 [16]. The absolute configuration of **3** was determined to be 5*S*, 10*R*, 13*R*, 14*R*, and 15*R* by comparing the experimental and calculated ECD spectra (Supplementary Fig. S34). Consequently, compound **3** was structurally elucidated as 14β,16-epoxy-15α-hydroxy-*ent*-pimar-8-en-3-one.

The known compounds 14β,16-epoxy-*ent*-3β,15α-dihydroxypimar-7-ene (**4**) [14], 14β,16-epoxy-*ent*-3β,15α,19-trihydroxypimar-7-ene (**5**), 14β,16-epoxy-*ent*-3α,15α,19-trihydroxypimar-7-ene (**6**) [17], 16β,17-dihydroxykauran-18-oic acid (**7**) [18], *ent*-kauran-16β,17,18-trio1 (**8**) [19], and 16β-hydro-*ent*-kauran-17,19-dioic acid (**9**) [20], were identified through analysis of their NMR data and comparison with published literature values.

2.2. Compound **5** inhibited cell death caused by high-glucose and IL-1β in HRECs

To evaluate compounds with protective effects against high glucose and IL-1β-induced injury in HRECs, an *in vitro* model was established using high glucose and IL-1β treatment. As detailed in Supplementary Fig. S41A, 40 $mmol \cdot L^{-1}$ high-glucose and 10 $ng \cdot mL^{-1}$ IL-1β were selected for subsequent experiments. Four compounds (**5**, and **7**–**9**) that exhibited higher concentrations

were selected for further investigation. Among these, compound **5** demonstrated the most significant protective effect on HRECs stimulated by high glucose and IL-1β, effectively preserving cell viability (Figs. 2A and 2B). Notably, compound **5** did not exhibit any significant cytotoxicity towards HRECs (Supplementary Fig. S41B). Under conditions of high glucose and IL-1β stimulation, *E*-cadherin distribution and expression were inhibited; however, compound **5** enhanced their distribution and expression levels (Figs. 2C, 2E and Supplementary Fig. S42A). Immunofluorescence with CD31 is a well-established technique to assess endothelium damage. As illustrated in Figs. 2D, 2F and Supplementary Fig. S42B, the protein level of CD31 was reduced in HRECs treated with high glucose and IL-1β, an effect reversed by compound **5**, as demonstrated by both immunofluorescence and Western blotting analyses.

The ERK, a mitogen-activated protein kinase, plays a critical role in promoting cell survival, proliferation, and angiogenesis [21]. Further investigation into ERK activity revealed that high glucose and IL-1β inhibited p-ERK activity, whereas compound **5** enhanced it (Fig. 2G).

Table 1 NMR spectroscopic data for compounds **1**–**3** (*J* in Hz) in $CDCl_3$ (^{1}H NMR: 600 MHz; ^{13}C NMR: 150 MHz).

No.	**1**		**2**		**3**	
	δ_C	δ_H	δ_C	δ_H	δ_C	δ_H
1	36.3	1.69 td (4.0, 13.2) 2.38 td (3.4, 13.2)	37.0	1.37 t (13.4) 2.23 m[b]	34.8	2.03 m[d] 1.60 m[e]
2	27.7	1.86 m[a]	24.5	1.86 m 2.20 dd (3.7, 13.4)	34.5	2.60 m 2.46 m[f]
3	78.3	3.35 d (11.4)	84.7	3.57 dd (4.2, 12.0)	217.5	
4	39.0		38.6		47.5	
5	48.7	1.85 m[a]	50.5	1.18 dd (1.8, 12.1)	51.2	1.67 m[g]
6	36.0	2.72 m	19.1	1.75 m 1.63 m	19.9	1.68 m[g] 1.61 m[e]
7	199.6		30.7	2.72 m 2.82 dd (6.2, 17.0)	30.5	2.48 m[f] 1.99 m
8	130.5		134.8		125.8	
9	152.7		147.0		139.8	
10	37.7		37.3		37.5	
11	124.0	7.24 d (8.1)	124.8	7.15 d (8.1)	20.9	2.02 m[d] 2.02 m[d]
12	135.2	7.35 dd (1.2, 8.1)	126.9	7.00 d (8.0)	29.3	1.35 m 1.35 m
13	136.2		134.5		43.1	
14	127.6	7.82 d (1.2)	129.7	6.83 s	82.5	3.61 s
15					80.3	3.89 brs
16					74.0	4.27 dd (5.0, 10.1) 3.66 dd (2.3, 10.1)
17	20.9	2.35 s	20.8	2.23 s[b]	18.9	1.12 s
18	27.6	1.06 s	28.5	1.24 s	21.4	1.08 s
19	15.1	0.97 s	16.8	0.96 s	26.7	1.12 s
20	23.6	1.24 s	25.0	1.12 s	14.4	0.97 s
1′			102.5	4.93 d (7.9)		
2′			75.2	4.04 t (7.9)		
3′			78.7	4.28 m[c]		
4′			72.0	4.26 m[c]		
5′			78.3	3.96 m		
6′			63.2	4.58 brd (12.0), 4.39 m		

[a–g] mean overlapping signals.

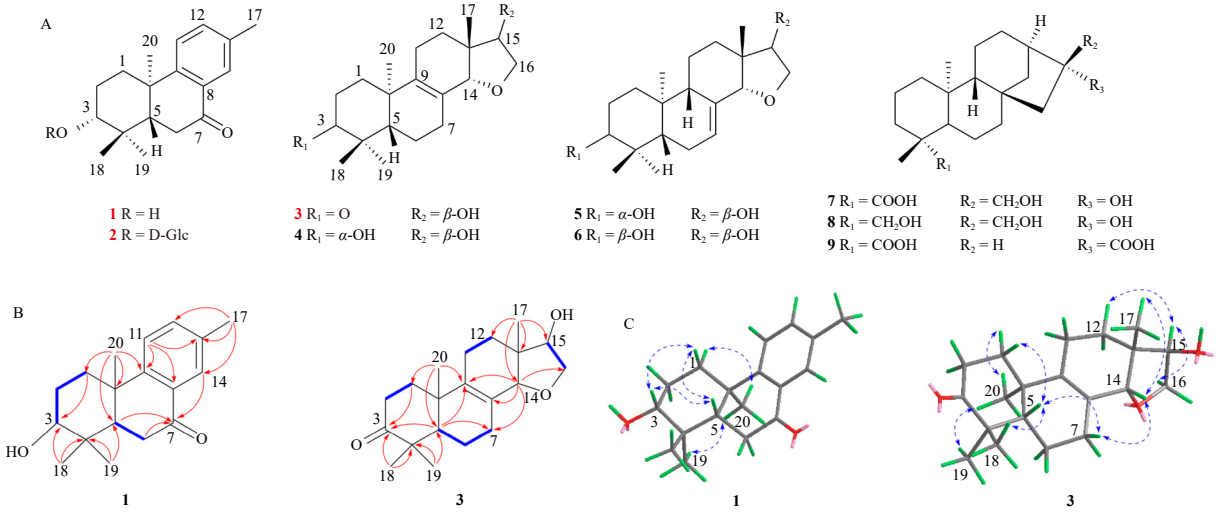

Fig. 1 Diterpenoid compounds **1**–**9** from *Siegesbeckia pubescens*. (A) Structures of compounds **1**–**9**. (B) Key ^{1}H–^{1}H COSY (▬) and HMBC (H⟶C) correlations of compounds **1** and **3**. (C) Key NOESY correlations of compounds **1** and **3**.

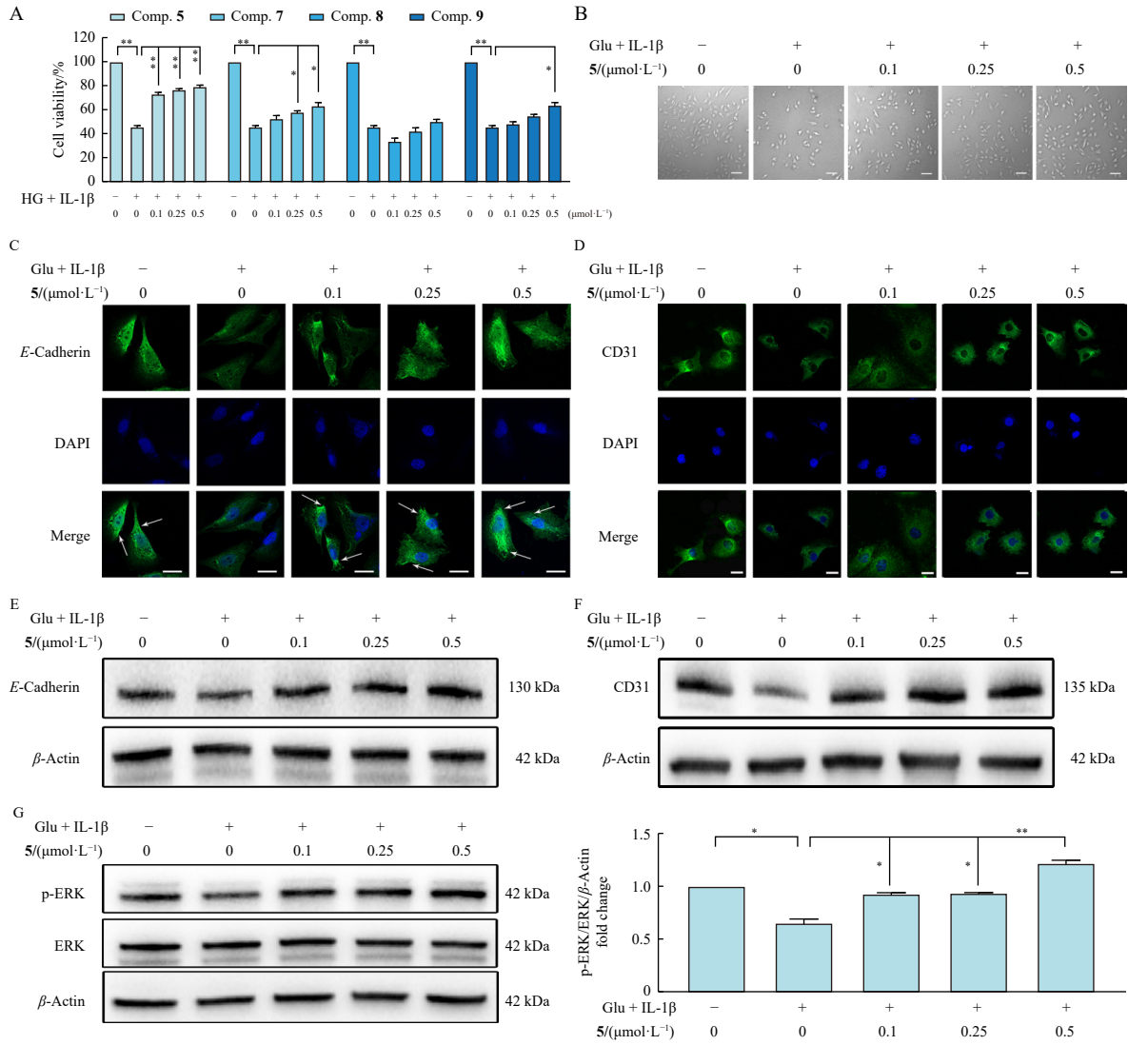

Fig. 2 Compound **5** inhibited cell death caused by high-glucose and IL-1β in HRECs. (A) HRECs were exposed to different concentrations of compounds (**5**, **7**–**9**) under high glucose and IL-1β conditions, and cell viability was measured by SRB assay. (B) HRECs were treated with compound **5** under high glucose and IL-1β conditions. After treatment for 48 h, representative phase-contrast microscopy images of HRECs were obtained (scale bars: 500 μm). (C) Representative immunofluorescence staining images for *E*-cadherin and DAPI in HRECs (scale bars: 100 μm). (D) HRECs were loaded with CD31 and DAPI and observed under a fluorescence microscope (scale bars: 200 μm). (E–G) The protein level of *E*-cadherin and CD31 and ERK/p-ERK was determined using western blot assays. Data are expressed as the mean ± SD (n = 3). $^{*}P < 0.05$, $^{**}P < 0.01$.

2.3. Compound **5** further investigation into ERK activity revealed that high glucose and IL-1β inhibited p-ERK activity, whereas compound **5** enhanced under high glucose and IL-1β conditions

To evaluate whether compound **5** promotes cell survival and proliferation through activation of the ERK signaling pathway, HRECs were treated with U0126, an inhibitor specifically targeting the ERK pathway. As illustrated in Figs. 3A and 3B, the observed increase in cell viability induced by compound **5** under high glucose and IL-1β conditions was effectively reversed upon administration of U0126. Moreover, *E*-cadherin expression was significantly inhibited after U0126 treatment, as demonstrated by immunofluorescence and Western blotting assays (Figs. 3C and 3E). Additionally, U0126 effectively blocked the up-regulation of CD31 expression (Figs. 3D and 3F). Collectively, these findings strongly suggest that the activation of the ERK signaling pathway is involved in compound **5**-induced cell proliferation.

2.4. Compound **5** attenuated cellular oxidation induced by high glucose and IL-1β

In a high glucose environment, vascular endothelial cells exhibit excessive production of mitochondrial ROS [22]. This ROS overload damages mitochondria, leading to capillary cell apoptosis and ultimately contributing to the development of DR. We subsequently examined ROS production in HRECs under high glucose and IL-1β conditions, with or without compound **5** treatment. As illustrated in Fig. 4A, both high glucose and IL-1β significantly increased intracellular ROS production compared to the control group; however, compound **5** treatment reversed these effects. Excessive oxidative stress can impair mitochondrial structure and function. Metalloproteinases 2 and 9 (MMP-2 and MMP-9), indicators of normal mitochondrial function, were assessed using the JC-1 probe. Fig. 4B shows that HRECs exposed to high glucose and IL-1β exhibited collapsed MMP, indicated by green

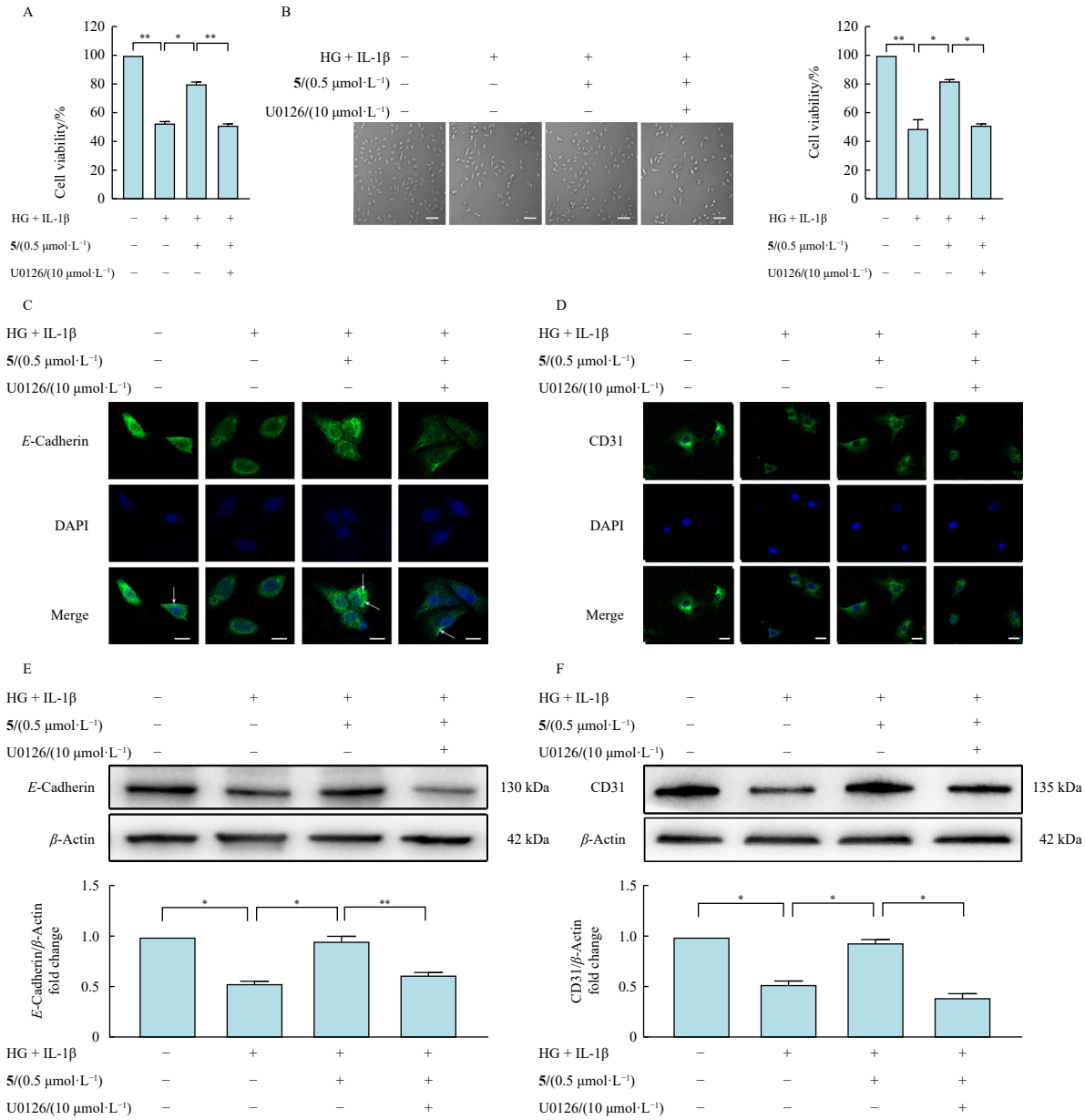

Fig. 3 Compound **5** promoted cell proliferation by activating ERK pathway under high glucose and IL-1β conditions. (A) HRECs were exposed to different concentrations of compound **5** with U0126 under high glucose and IL-1β conditions, and cell viability was tested using SRB assay. (B) HRECs were co-treated with compound **5** and U0126 under high glucose and IL-1β conditions. After treatment for 48 h, representative phase-contrast microscopy images of HRECs were obtained (scale bars: 500 μm). (C) Representative immunofluorescence staining images for *E*-cadherin and DAPI in HRECs co-treated with compound **5** and U0126 under high glucose and IL-1β conditions (scale bars: 100 μm). (D) HRECs were loaded with CD31 and DAPI and observed under a fluorescence microscope (scale bars: 200 μm). (E and F) The protein levels of *E*-cadherin and CD31 in HRECs were detected by western blot assays. Data are expressed as the mean ± SD ($n = 3$). $^{*}P < 0.05$, $^{**}P < 0.01$.

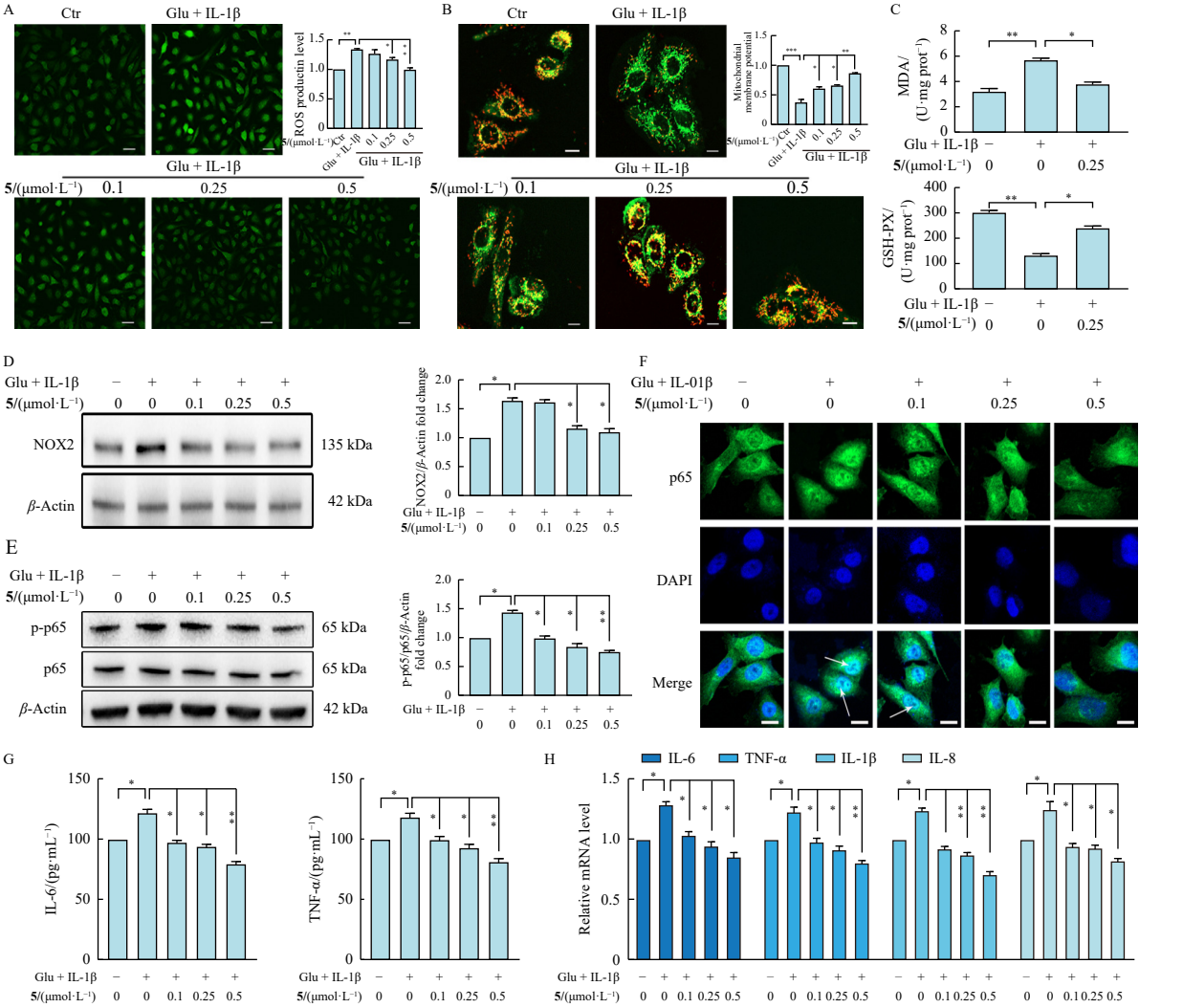

Fig. 4 Compound **5** attenuated cellular oxidation and inflammatory responses induced by high glucose and IL-1β. (A) ROS level was determined by DCFH-DA after 48 h treatment of compound **5** with high glucose and IL-1β (scale bars: 100 μm). (B) The mitochondrial membrane potential was observed using the JC-1 detection kit by fluorescence microscope (scale bars: 50 μm). (C) The content of MDA and GSH-PX were measuerd using malondialdehyde assay kit. (D)The protein level of NOX2 was tested using western blot assays. *β*-actin was used for normalization. (E) The protein level of p-p65/p65 were detected by western blot. (F) Representative immunofluorescence staining images for p65 and DAPI in HRECS treated with or without compound **5** under high glucose and IL-1β conditions (scale bars: 100 μm). (G) The content of IL-6 and TNF-α was measured using ELISA. (H) The mRNA expression levels of IL-1β, IL-6, IL-8 and TNF-α were detected using PCR assay in HRECs with different concentrations of compound **5** for 24 h. Data are expressed as the mean ± SD ($n = 3$). $^{*}P < 0.05$, $^{**}P < 0.01$, $^{***}P < 0.001$.

fluorescence; conversely, cells treated with compound **5** displayed orange fluorescence. Furthermore, compound **5** significantly reduced NOX2 expression compared to the high glucose and IL-1β group (Fig. 4D). Additionally, compound **5** demonstrated a protective effect on MDA levels and GSH-PX activity in HRECs under high glucose and IL-1β conditions (Fig. 4C). These findings collectively indicate that compound **5** effectively protected HRECs against oxidative stress induced by high glucose and IL-1β.

*2.5. Compound **5** mitigated inflammatory responses induced by high glucose and IL-1β*

To validate the anti-inflammatory activity of compound **5** in HRECs under high glucose and IL-1β conditions, its effects on NF-κB activation were evaluated. Western blotting and immunofluorescence analyses demonstrated that compound **5** significantly counteracted p-p65 protein levels and p65 nuclear translocation, both indicators of NF-κB activity (Figs. 4E and 4F). Additionally, compound **5** markedly suppressed the protein secretion of IL-6 and TNF-α following the combined stimulus (Fig. 4G). Furthermore, the simultaneous incubation with high glucose and IL-1β increased IL-6, TNF-α, IL-8, and IL-1β mRNA expression, all of which were inhibited by compound **5** (Fig. 4H). These results indicate that compound **5** mitigated inflammatory responses in HRECs stimulated by high glucose and IL-1β.

*2.6. Compound **5** attenuated diabetes-induced oxidative stress and inflammatory responses in vivo*

To thoroughly investigate the effects of compound **5**, we utilized a murine model of type 2 diabetes mellitus (T2DM) to assess its *in vivo* efficacy. Elevated blood glucose levels and weight loss are recognized as primary indicators of diabetes. Our results revealed that treatment with compound **5** (DM + L, DM + H) effectively mitigated body weight reduction and attenuated the increase in blood glucose levels compared to the DM group (Figs. 5A and 5B). After an 8-week administration of compound **5**, significant inhibition of MDA levels and enhancement of GSH-PX levels were observed relative to the DM group (Figs. 5C and 5D). Additionally, a notable reduction in pro-inflammatory cytokines IL-6 and TNF-α was detected in serum samples (Figs. 5E and 5F). As illustrated in Fig. 5G, compared to the DM group, compound **5** treatment successfully ameliorated aortic wall thickening in both

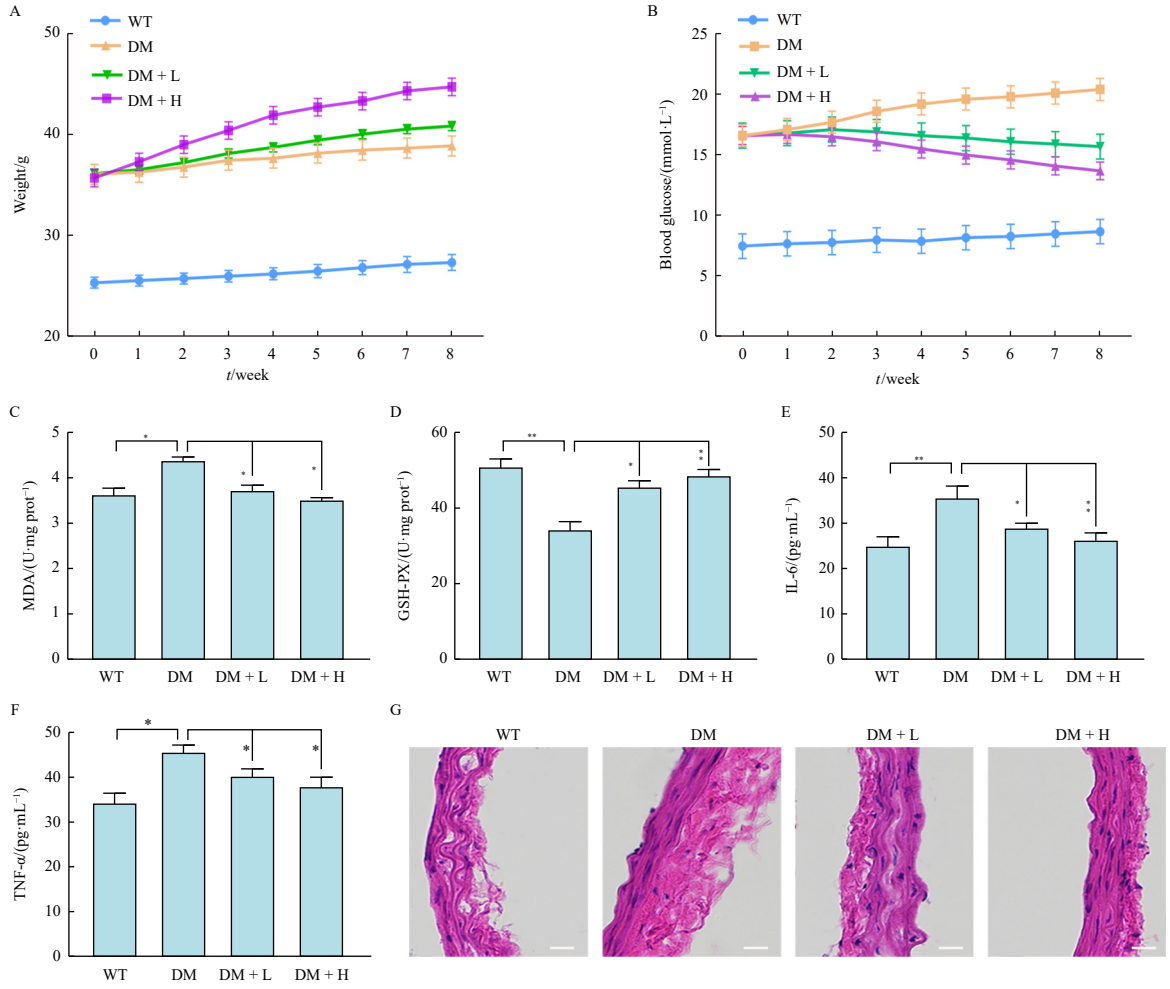

Fig. 5 Compound **5** attenuated diabetes-induced oxidative stress and inflammatory responses *in vivo*. (A) Diabetic mice were intervented with compound **5** ((DM + L: 1 mg·kg^{-1}, DM + H: 2 mg·kg^{-1}) for 8 weeks and the weight were measured every week. (B) The blood glucose of diabetic mice was tested every week. (C and D) At the end of the experiment, the level of MDA and GSH-PX in serum were determined by commercial kits. (E and F) The content of IL-6 and TNF-α were assessed in serum at the end of experiment. (G) Diabetic mice were treated with compound **5** (DM + L: 1 mg·kg^{-1}, DM + H: 2 mg·kg^{-1}) for 8 weeks and H&E staining were preformed (scale bars: 200 μm). Data were presented as the mean ± SD (n = 6). $^{*}P < 0.05$, $^{**}P < 0.01$.

DM + L and DM + H groups.

3. Discussion

Siegesbeckia pubescens Makino has been reported to possess various pharmacological effects, including anti-inflammatory and analgesic properties. It has also demonstrated potential in treating hypertension, stroke, and a variety of inflammatory diseases. However, the biological potential of *S. pubescens* in oxidative stress and inflammatory responses in DR remains unexplored. In this study, we extracted nine compounds from the aerial parts of *S. pubescens*, which included three novel *ent*-pimarane-type diterpenoids (**1**–**3**) along with six known compounds (**4**–**9**). Furthermore, our findings indicated that 14*β*,16-epoxy-*ent*-3*β*,15*α*,19-trihydroxypimar-7-ene (**5**) exhibited the most potent protective effect against high glucose and IL-1β-stimulated HRECs, demonstrating its antioxidant and anti-inflammatory effects both *in vivo* and *in vitro*.

Hyperglycemia and inflammatory cytokines are potential mechanisms inducing vascular endothelial dysfunction and damage during the development of DR. This study initially established an *in vitro* injury model of HRECs using 40 mmol·L^{-1} high glucose and 10 ng·mL^{-1} IL-1β, based on previous research demonstrating that high glucose and IL-1β could trigger endothelial injury in HUVECs [23]. As previously noted, one characteristic of DR is reduced endothelial cell survival. Furthermore, the progressive dysfunction of endothelial cells contributes to pathophysiological changes in the retina [24]. Consequently, protecting retinal endothelial cells from injury is crucial in delaying the progression of diabetic retinal diseases. Compound **5** demonstrated protective effects against HREC death induced by glucose and IL-1β while simultaneously promoting the expression of *E*-cadherin and CD31. During these processes, ERK, a key protein kinase associated with an important signaling pathway, was activated. Notably, U0126, an inhibitor of the ERK pathway, was found to compromise the protective effects of compound **5**.

In the retina, chronic hyperglycemia renders microvessels susceptible to oxidative stress, leading to increased generation of ROS [25], which plays a central role in the development of DR [26]. Mitochondria are a key source of ROS production. Additionally, in the pathogenesis of DR, ROS are produced in the cytosol by NOX2. Notably, excess ROS production further impairs mitochondrial function. Our studies demonstrated that compound **5** reversed the excess production of intracellular ROS and inhibited NOX2 activity. Furthermore, compound **5** protected mitochondrial function in high glucose and IL-1β environments. Research has shown that in retinal cells, excess ROS can upregulate matrix MMP-2 and MMP-9, which impair mitochondrial membrane potential, leading to apoptosis. It is well-established that MMPs can cleave *E*-cadherin at the cell surface [27,28]. Based on published research and our findings that compound **5** inhibits ROS production, recovers mitochondrial membrane potential, and enhances *E*-cadherin ex-

pression and distribution, we hypothesize that compound **5** may also suppress MMP activity in HRECs.

Moreover, research has demonstrated that the disequilibrium between ROS production and antioxidant defense mechanisms activates pathways associated with oxidative stress, thereby promoting the onset of DR [29]. Our findings indicate that compound **5** exhibits the potential to enhance the synthesis of GSH-PX while simultaneously reducing the concentration of MDA.

Persistent elevated glucose levels in circulation not only increase oxidative stress but also trigger an inflammatory cascade in the retina [30]. Substantial evidence confirms that chronic inflammation plays a crucial role in the development of DR, particularly in its early stages. NF-κB, a ubiquitous transcription factor, activates inflammatory mediators, enhances oxidative stress, and contributes to the pathogenesis of DR [25, 30, 31]. Consequently, modulating NF-κB activation presents a potential treatment strategy for DR. Studies have demonstrated that inhibition of NF-κB activation could mediate the suppression of early capillary degeneration in DR [32]. Moreover, chronic hyperglycemia in DR patients leads to increased production of pro-inflammatory cytokines, including TNF-α and IL-1β, resulting in subsequent destruction of retinal cells [33, 34]. Our data indicate that high glucose and IL-1β activated NF-κB, promoted its nuclear translocation, and increased the expression of IL-6, TNF-α, IL-1β, and IL-8. Compound **5** significantly inhibited NF-κB activation and the subsequent production of IL-6, TNF-α, IL-1β, and IL-8. Furthermore, to investigate the antioxidant and anti-inflammatory effects of compound **5** *in vivo*, experiments were conducted on diabetic mice. The results demonstrated that treatment with compound **5** *in vivo* also exerted antioxidant and anti-inflammatory effects.

4. Conclusion

In summary, diterpenoids such as 14*β*,16-epoxy-*ent*-3*β*,15*α*,19-trihydroxypimar-7-ene (**5**) serve as crucial anti-inflammatory components in *S. pubescens*. These compounds demonstrate the capacity to mitigate oxidative stress and inflammatory responses both *in vivo* and *in vitro* (Fig. 6). This finding not only presents potential new drug candidates but also offers novel therapeutic avenues for the application of *S. pubescens* in the treatment of DR.

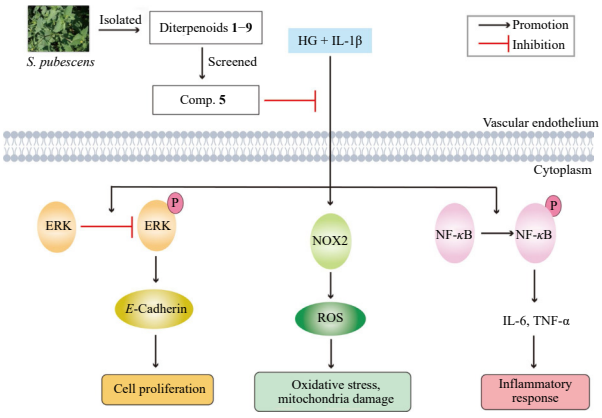

Fig. 6 The schematic diagram of the key function of compound **5** in diabetic retinopathy. Compound **5** attenuated the retinal endothelium injury induced by high glucose and IL-1β *via* regulating ERK/NF-κB.

5. Experimental

5.1. General experimental procedures

Optical rotation was measured using a Rudolph VI polarimeter (Rudolph Research Analytical, Hackettstown, NJ, USA). ECD spectra were recorded on a Chirascan CD spectropolarimeter (Applied Photophysics Ltd., Surrey, UK). Ultraviolet (UV) and infrared spectroscopy (IR) data were obtained using a Shimadzu UV-2600 spectrophotometer (Shimadzu, Kyoto, Japan) and VERTEX70 spectrometer (Bruker Optics Inc., Billerica, USA), respectively. NMR experiments were conducted on a Bruker Avance DRX-600 spectrometer (Bruker BioSpin AG, Fällanden, Switzerland) and referenced to residual solvent signals ($CDCl_3$: δ_H 7.26, δ_C 77.16). ESI-MS and HR-ESI-MS analyses were performed on Agilent 6460 Triple Quad liquid chromatography-mass spectrometry (LC/MS) and Agilent 6545 Q-TOF LC/MS spectrometers (Agilent Technologies Inc., Waldbronn, Germany), respectively. Column chromatography (CC) was carried out using D101-macroporous absorption resin (Sinopharm Chemical Reagent Co., Ltd., Shanghai, China), Silica gel (200–300 mesh, Qingdao Marine Chemical Plant Ltd., Qingdao, China), Sephadex LH-20 (GE Healthcare Bio-Sciences AB, Uppsala, Sweden), MCI gel (CHP20P, Mitsubishi Chemical Corporation, Tokyo, Japan) and reversed-phase C_{18} silica gel (Merck KGaA, Darmstadt, Germany). Precoated silica gel GF254 plates (Yantai Jiangyou Silica Gel Development Co., Yantai, China) were utilized for thin-layer chromatography (TLC). Semi-preparative high-performance liquid chromatography (HPLC) was conducted on an Agilent 1260 series liquid chromatography (LC) instrument (Agilent Technologies Inc., Waldbronn, Germany) equipped with an octadecylsilyl (ODS) column (YMC-pack ODS-A, 10 mm × 250 mm, 5 μm). All solvents used for CC were of analytical grade (Tianjin Fuyu Fine Chemical Co., Ltd., Tianjin, China), and solvents used for HPLC were of HPLC grade (Oceanpak Alexative Chemical Ltd., Goteborg, Sweden).

5.2. Plant material

The aerial components of *S. pubescens* were procured from the Materia Medica Market in Kunming City, Yunnan Province, China, in September 2018. Dr. Fengying Yang from the University of Jinan authenticated the specimen. A voucher specimen has been deposited at the School of Biological Science and Technology, University of Jinan (Accession number: NPVS-20180924).

5.3. Extraction and isolation

Air-dried powdered plant material (10.0 kg) was percolated three times (3 × 100 L, each for one week) with 95% EtOH at room temperature. The crude extract (639.0 g) was suspended in H_2O (1.5 L) and extracted with EtOAc (4 × 1.5 L). The EtOAc partition (306.0 g) was separated by CC over D101-macroporous absorption resin, eluted with MeOH–H_2O (50%, 80%, 95%, 100%) to yield four fractions (Fr.1–Fr.4). Fr.1 (53.6 g) was applied to a silica gel (200–300 mesh) column using petroleum ether–acetone (8∶1, 4∶1, 2∶1, 1∶1) as eluent to afford seven fractions (Fr.1.1–Fr.1.7). Fr.1.3 (20.6 g) was first subjected to silica gel CC eluted with $CHCl_3$–MeOH (1∶0 to 1∶1) and then subjected to an ODS column using MeOH–H_2O (from 30∶70 to 90∶10, *V/V*) as the elution system to afford eight fractions (Fr.1.3.1–Fr.1.3.8). Fr.1.3.4 (42.0 mg) was purified by HPLC (82% MeOH–H_2O, 2.0 mL·min^{-1}) to obtain compound **7** (1.5 mg, t_R = 11.4 min). Fr.2 (44.1 g) was separated on a MCI gel column (MeOH–H_2O, 50∶50 to 95∶5, *V/V*) to yield three subfractions (Fr.2.1–Fr.2.3). Fr.2.3 (13.0 g) was then applied to a silica gel (200–300 mesh) column using petroleum ether–acetone (100∶1–1∶1, *V/V*) as eluent to afford seven fractions (Fr.2.3.1–Fr.2.3.7). Fr.2.3.5 (240.0 mg) was then purified by HPLC (63% MeCN–H_2O, 2.0 mL·min^{-1}) to obtain compound **9** (35.0 mg, t_R = 10.1 min). Fr.3 (25.6 g) was applied to a silica gel (300–400 mesh) CC using petroleum ether–acetone (100∶1–1∶2, *V/V*) as eluent to afford six fractions (Fr.3.1–Fr.3.6).

Fr.3.5 (14.2 g) was subjected to an ODS column using MeOH–H_2O (20∶80 to 90∶10, *V/V*) as the elution system to afford seven fractions (Fr.3.5.1–Fr.3.5.7). Fr.3.5.1 (156.0 mg) was further purified by preparative HPLC (MeOH–H_2O, 65∶35, *V/V*) to obtain compounds **4** (5.0 mg, t_R = 18.0 min), **5** (122.1 mg, t_R = 19.0 min), and **6** (3.2 mg, t_R = 21.7 min). Fr.3.5.3 (621.0 mg) was purified by semi-preparative HPLC (55% MeOH–H_2O, 2.0 mL·min^{-1}) to afford compound **3** (0.8 mg, t_R = 27.2 min). Fr.3.5.5 (461.0 mg) was purified by semi-preparative HPLC (67% MeOH–H_2O, 2.0 mL·min^{-1}) to afford compound **1** (2.0 mg, t_R = 11.3 min). Fr.4 (41.8 g) was applied to a silica gel (300–400 mesh) CC eluting with petroleum ether–acetone (10∶1–0∶1, *V/V*) as eluent to afford six fractions (Fr.4.1–Fr.4.6). Fr.4.3 (5.2 g) was subjected to an RP-18 column (MeOH–H_2O, from 70% to 100%, *V/V*) and further purified by preparative HPLC (80% MeOH–H_2O, 2.0 mL·min^{-1}) to yield **8** (1.5 mg, t_R = 15.7 min). Fr.4.5 (12.8 g) was separated by silica gel CC eluted with a gradient system of $CHCl_3$–MeOH (20∶1, 10∶1, 5∶1, 2∶1, 1∶2, *V/V*) to afford five subfractions (Fr.4.5.1–Fr.4.5.5). Fr.4.5.2 (2.2 g) was submitted to a MCI column using MeOH–H_2O (30∶70 to 85∶15, *V/V*) as eluent to afford five fractions (Fr.4.5.2.1–Fr.4.5.2.5). Fr.4.5.2.3 (90.2 mg) was further purified by semi-preparative HPLC (85% MeOH–H_2O, 2.0 mL·min^{-1}) to yield **2** (0.6 mg, t_R = 22.0 min).

3*β*-Hydroxy-15-devinyl-*ent*-pimar-8,11,13-triene-7-one (**1**): amorphous powder; $[\alpha]_D^{20}$ +2.5 (*c* 0.10, MeOH); UV (MeOH) λ_{max} (log ε) 210 (4.42), 251 (3.90) nm; IR (KBr) ν_{max} 3435, 2925, 2854, 1632, 1117 cm^{-1}; ECD (MeOH) λ ($\Delta\varepsilon$) 211 (−2.08), 253 (0.69), 297 (0.71), 327 (−1.21) nm; ^{13}C and ^{1}H NMR data, see Table 1; (+)-ESI-MS *m/z* 295.1 [M + Na]$^+$; (+)-HR-ESI-MS m/z 273.1841 [M + H]$^+$ (Calcd. for $C_{18}H_{24}O_2H$, 273.1849).

15-Devinyl-*ent*-pimar-8,11,13-triene-7-one-3*β*-*O*-*β*-D-glucopyranoside (**2**): amorphous powder; $[\alpha]_D^{20}$ −240.5 (*c* 0.10, MeOH); UV (MeOH) λ_{max} (log ε) 204 (4.47) nm; IR (KBr) ν_{max} 3432, 2926, 1623, 1075, 1029 cm^{-1}; ECD (MeOH) λ ($\Delta\varepsilon$) 201 (−2.99) nm; ^{13}C and ^{1}H NMR data, see Table 1; (+)-ESI-MS *m/z* 443.1 [M + Na]$^+$; (+)-HR-ESI-MS *m/z* 443.2401 [M + Na]$^+$ (Calcd. for $C_{24}H_{36}O_6Na$, 443.2404).

14*β*,16-Epoxy-15*α*-hydroxy-*ent*-pimar-8-en-3-one (**3**): amorphous powder; $[\alpha]_D^{20}$ −8.0 (*c* 0.10, MeOH); UV (MeOH) λ_{max} (log ε) 205 (4.33) nm; IR (KBr) ν_{max} 3432, 2925, 2361, 1702, 1621 cm^{-1}; ECD (MeOH) λ ($\Delta\varepsilon$) 217 (0.34), 301 (0.38) nm; ^{13}C and ^{1}H NMR data, see Table 1; (+)-ESI-MS *m/z* 341.2 [M + Na]$^+$; (+)-HR-ESI-MS *m/z* 319.2258 [M + H]$^+$ (Calcd. for $C_{20}H_{30}O_3H$, 319.2268).

5.4. Reagents and antibodies

IL-1β protein was obtained from Abclonal (RP00002, Wuhan, China). Antibodies against CD31 (A19014), NOX2 (A19701), p65 (A19653), and p-p65 (AP0124) were acquired from Abclonal (Wuhan, China). *β*-Actin (sc-47778) and biotinylated goat anti-rabbit IgG (BA-1000) antibodies, as well as anti-rabbit IgG (sc-2004) and HRP-conjugated anti-mouse IgG (sc-2371) secondary antibodies, were sourced from Santa Cruz Biotechnology (Santa Cruz, CA, USA).

5.5. Cell culture

HRECs were acquired from Cell Systems, Inc. (Shanghai, China) and cultivated in DMEM (Thermo Fisher Scientific, Shanghai, China) supplemented with 5% fetal bovine serum (Thermo Fisher Scientific, Shanghai, China). The cells were maintained at 37 °C in a humidified CO_2 incubator with an atmosphere composed of 95% air and 5% CO_2.

5.6. Animals experiment

All animal care and experimentation were conducted in accordance with the guidelines for Animal Experimentation of University of Jinan (Jinan, China) and approved by the Science and Technology Ethics Committee of University of Jinan. The approval number for the Science and Technology Ethics Review is UJNBIO-2023-008. Wild-type male C57BL/6 mice and *db/db* mice (C57BL/6-lepr^{db}/lepr^{db}) with the same background (7 weeks old) were obtained from Hangzhou Ziyuan Experimental Animal Technology Co., Ltd. (Hangzhou, China). Male C57BL/6 mice and *db/db* mice were maintained under standard conditions according to approved protocols. Diabetic mice (*db/db*) were randomly assigned to 3 groups: DM group (1% DMSO saline, *n* = 6), DM + L group (1 mg·kg^{-1} compound **5**, dissolved in saline containing 1% DMSO, *n* = 6), DM + H group (2 mg·kg^{-1} compound **5**, dissolved in saline containing 1% DMSO, *n* = 6). Six C57BL/6 mice were administered normal saline containing 1% DMSO as a normal control. The four groups of mice received intragastric administration once every two days for eight weeks. Subsequently, the mice were euthanized and weighed, and serum was collected for further experiments.

5.7. Cell viability assay

The viability of HRECs was assessed using the sulforhodamine B (SRB, MACKLIN, Shanghai, China) assay. In brief, 3 × 10^3 HRECs were seeded into 96-well plates. Subsequently, cells were exposed to glucose and IL-1β, with or without compound **5** (0.1, 0.25, 0.5 μmol·L^{-1}) for 24 h. Absorbance at 540 nm was measured using a microplate reader (TECAN, Switzerland). Results were expressed as cell viability percentage. Cell survival rate (%) was calculated as (Experimental − Blank)/(Control − Blank) × 100%. The experiment was conducted in triplicate.

5.8. GSH-PX assay

HRECs (1 × 10^5/mL) in the exponential growth phase were seeded into 60 mm dishes and incubated overnight. Subsequently, the cells were exposed to compound **5** or high glucose and IL-1β for 24 h, after which they were harvested. The cells were resuspended in 0.3–0.5 mL phosphate-buffered saline (PBS) and lysed by sonication for analysis. Reagents were added to the cell lysate according to the manufacturer's instructions. The suspension was then centrifuged at 8000 r·min^{-1} for 10 min, and the supernatant was collected for testing. The protein content of HRECs was determined using a bicinchoninic acid assay (BCA) kit (PC0020, Solaibio, Beijing, China). Absorbance was measured at 405 nm using a microplate reader. The GSH-PX (A005, Nanjing Jiancheng Bioengineering Research Institute, Nanjing, China) content in HRECs was calculated using the following formula: GSH-PX (U·mg prot^{-1}) = [(Tested − Blank)/(Standard − Blank)] × 40 μmol·L^{-1}/protein concentration (g prot·L^{-1}).

5.9. MDA assay

MDA is considered a crucial marker of lipid peroxidation. The total quantities of MDA were determined using an MDA assay kit (BC0025, Solarbio, Beijing, China). HRECs were processed according to the manufacturer's instructions, and reagents were added as recommended. The mixture was subjected to a water bath at 100 °C for 60 min, cooled in an ice bath, and subsequently centrifuged for 10 min at 10 000 r·min^{-1}. The supernatant was then harvested, and 200 μL was transferred to a 96-well plate. Absorbance readings for each sample were recorded at 450, 532 and 600 nm. The following calculations were performed: $\Delta A_{450} = A_{450\ (Test)} - A_{450\ (Blank)}$, $\Delta A_{532} = A_{532\ (Test)} - A_{532\ (Blank)}$, $\Delta A_{600} = A_{600\ (Test)} - A_{600\ (Blank)}$. The MDA content was calculated relative to the protein concentration, determined using a BCA kit. The final MDA concentration was expressed as U·mg prot^{-1} and calculated

using the formula: 5 × [12.9 × (ΔA_{532} − ΔA_{600}) − 2.58 × ΔA_{450}]/Cpr.

5.10. ROS assay

HRECs (1 × 10^6 cells/well) were co-cultured with compound **5** under high glucose and IL-1β conditions for 24 h. Subsequently, DCFH-DA (S0033S, Beyotime, Shanghai, China) was added to each well with a serum-free medium and incubated at 37 °C for an additional 20 min. The cells were washed twice with serum-free medium. Following cell collection, the fluorescence changes in HRECs were observed *via* a fluorescence microscope at 488/525 nm. The fluorescence intensity was quantified using Image J software through densitometric analysis.

5.11. Detection of the mitochondrial membrane potential (MMP)

HRECs (1 × 10^6 cells/well) were co-cultured with compound **5** following high glucose and IL-1β stimulation. Subsequently, the cells were washed twice with PBS and treated with 100 μL of JC-1 (P10009908, Cayman, Beijing, China) staining solution per mL of culture medium in each well of the plate. After incubating samples in a CO_2 incubator at 37 °C for 30 min, fluorescence changes in HRECs were observed using a fluorescence microscope. JC-1 accumulated in the mitochondrial matrix, producing red fluorescence when excited at wavelengths of 585/590 nm; alternatively, JC-1 remained in its monomer form and generated green fluorescence at wavelengths of 514/529 nm. The red and green fluorescence signals merged to produce orange fluorescence. The intensity of fluorescence was quantified by densitometry using Image J software.

5.12. Quantitative real-time PCR (qRT-PCR)

Total RNA was extracted using TRIzol reagent (Invitrogen, Carlsbad, CA, USA) following the manufacturer's protocol. RT-PCR was conducted to assess mRNA expression using the following primers: human IL-1β (forward, 5'-CTCTTCGAGGCACAAGGCAC-3'; reverse, 5'-TGGCTGCTTCAGACACTTGAG-3'), human IL-6 (forward, 5'-TGAGGAGACTTGCCTGGTGA-3'; reverse, 5'-CACAGCTCTGGCTTGTTCCT-3'), human IL-8 (forward, 5'-TCTGCAGCTCTGTGTGAAGG-3'; reverse, 5'-TGGGGTGGAAAGGTTTGGAG-3'), human TNF-α (forward, 5'-TGTCTACTGAACTTCGGGGTGAT-3'; reverse, 5'-AACTGATGAGAGGGAGGCCAT-3'), *β*-Actin (forward, 5'-AAGTGTGACGTGGACATCCG-3'; reverse, 5'-TTCTGCATCCTGTCGGCAAT-3'). A 4.4 μL aliquot of cDNA was amplified *via* RT-PCR in a total volume of 10 μL. The RT-PCR procedure consisted of an initial denaturation step at 95 °C for 30 min, followed by 40 cycles of standard PCRR.

5.13. ELISA

The concentrations of IL-6 (PK00004, Abclonal, Wuhan, China) and TNF-α (PK00030, Abclonal, Wuhan, China) in the blood samples obtained during the animal study were quantified using commercially available kits, in accordance with the manufacturers' instructions.

HRECs (1 × 10^6) were seeded into 6-well plates and cultured until reaching 70%–80% confluence. After washing with PBS, cells were exposed to high glucose and IL-1β, followed by incubation with or without compound **5** for 24 h. The cell supernatant was collected, and the concentrations of IL-6 and TNF-α in the culture supernatant were quantified using an ELISA kit according to the manufacturer's protocol. The final concentrations of IL-6 and TNF-α were determined by converting optical density (OD) readings based on standard curves.

5.14. Immunofluorescence assay

Immunofluorescence staining was conducted following the protocol outlined in reference [35]. HRECs were cultured in a dish and exposed to compound **5** or a combination of high glucose and IL-1β for 24 h. Subsequently, the cells were fixed with 4% paraformaldehyde at room temperature for 15 min, washed thrice with PBS for 10 min each, and blocked with 1% goat serum in PBS at room temperature for 1 h. Following another three washes with PBS, the cells were incubated overnight at 4 °C with primary CD31 antibody. The cells were then incubated with the corresponding secondary antibody at 37 °C for 1 h before being examined under a fluorescence microscope.

5.15. Western blotting analysis

HRECs from passage 6 were cultured to 70%–80% confluence. Following compound treatment, cells were lysed at 4 °C using lysis buffer. The lysates were centrifuged at 12 000 × *g* for 15 min at 4 °C, and protein concentrations were determined. Lysed whole-cell proteins were mixed with 0.02% bromophenol blue and boiled for 5 min. Subsequently, 15–20 μg of total protein extracts were separated using SDS-PAGE. The separated proteins were transferred to a PVDF membrane (Millipore, ISEQ09120). The membrane was blocked with 5% nonfat dry milk in TBST for 1 h, then incubated with primary antibodies at 4 °C for 16 h. After three 5-min rinses with TBST, the membrane was incubated with HRP-conjugated secondary antibodies for 1 h at 25 °C. Immunoreactive bands were visualized using Pierce ECL (32106, Thermo Fisher Scientific, Shanghai, China) Western blot substrate. Relative protein levels were quantified using Image J software.

5.16. H&E staining

Following 24-h fixation in 4% paraformaldehyde, the tissue was embedded in paraffin. The paraffin was subsequently removed by xylene immersion for 10 min. The tissue was then stained with hematoxylin solution for 15 min, rinsed under running water for 30 min, and counterstained with eosin for 30 s, resulting in pink-stained cytoplasm. After rinsing with running water, the tissue was again immersed in xylene for 10 min. Finally, microscopic images were captured for analysis.

5.17. Statistical analysis

Data were presented as means ± standard deviation (SD). Statistical analysis was performed using GraphPad Prism V6.0 (La Jolla, CA, USA). All error bars represent standard deviation (n = 3) unless otherwise specified. Statistical significance was determined at $P \leq 0.05$.

Funding

This research was supported by the National Natural Science Foundation of China (No. 82073728) and the Natural Science Foundation of Shandong Province (No. ZR2021MH357).

Supplementary information

Supporting information for this study can be obtained by contacting the corresponding authors *via* E-mail.

Declaration of competing interest

These authors have no conflict of interest to declare.

References

1 Cecilia OM, Jose-Alberto CG, Jose NP, et al. Oxidative stress as the main target in diabetic retinopathy pathophysiology. *J Diabetes Res*. 2019;14:8562408. https://doi.org/10.1155/2019/8562408.
2 Kang Q, Yang C. Oxidative stress and diabetic retinopathy: molecular mechanisms, pathogenetic role and therapeutic implications. *Redox Biol*. 2020;37:101799. https://doi.org/10.1016/j.redox.2020.101799.
3 Imamura M, Takahashi A, Matsunami M, et al. Genome-wide association studies identify two novel loci conferring susceptibility to diabetic retinopathy in Japanese patients with type 2 diabetes. *Hum Mol Genet*. 2021;30(8):716–726. https://doi.org/10.1093/hmg/ddab044.
4 Nawaz IM, Rezzola S, Cancarini A, et al. Human vitreous in proliferative diabetic retinopathy: characterization and translational implications. *Prog Retin Eye Res*. 2019;72:100756. https://doi.org/10.1016/j.preteyeres.2019.03.002.
5 Moon CH, Lee AJ, Jeon HY, et al. Therapeutic effect of ultra-long-lasting human C-peptide delivery against hyperglycemia-induced neovascularization in diabetic retinopathy. *Theranostics*. 2023;13(8):2424–2438. https://doi.org/10.7150/thno.81714.
6 Wang M, Sheng K, Fang J, et al. Redox signaling in diabetic retinopathy and opportunity for therapeutic intervention through natural products. *Eur J Med Chem*. 2022;15(244):114829. https://doi.org/10.1016/j.ejmech.2022.114829.
7 National Pharmacopoeia Committee. *Pharmacopoeia of China*. China Med Sci Technol Press, 2015:368.
8 Sun Z, Zhang Y, Zhou H, et al. Diverse diterpenoids and sesquiterpenoids from *Siegesbeckia pubescens* and their activity against RANKL-induced osteoclastogenesis. *Bioorg Chem*. 2021;107:104537. https://doi.org/10.1016/j.bioorg.2020.104537.
9 Wang Z, Zhu S, Wu Z, et al. Kirenol upregulates nuclear annexin-1 which interacts with NF-κB to attenuate synovial inflammation of collagen-induced arthritis in rats. *J Ethnopharmacol*. 2011;137(1):774–782. https://doi.org/10.1016/j.jep.2011.06.037.
10 Wang J, Zhou Y, Ye, X, et al. Topical anti-inflammatory and analgesic activity of kirenol isolated from *Siegesbeckia orientalis*. *J Ethnopharmacol*. 2011;137(3):1089–1094. https://doi.org/10.1016/j.jep.2011.07.016.
11 Wu B, Huang X, Li L, et al. Attenuation of diabetic cardiomyopathy by relying on kirenol to suppress inflammation in a diabetic rat model. *J Cell Mol Med*. 2019;23(11):7651–7663. https://doi.org/10.1111/jcmm.14638.
12 Pracht P, Bohle F, Grimme S. Automated exploration of the low-energy chemical space with fast quantum chemical methods. *Phys Chem Chem Phys*. 2020;22(14):7169–7192. https://doi.org/10.1039/C9CP06869D.
13 Wang R, Chen W, Shi Y. *Ent*-kaurane and *ent*-pimarane diterpenoids from *Siegesbeckia pubescens*. *J Nat Prod*. 2010;73(1):17–21. https://doi.org/10.1021/np9005579.
14 Wang F, Cheng X, Li Y, et al. *Ent*-pimarane diterpenoids from *Siegesbeckia orientalis* and structure revision of a related compound. *J Nat Prod*. 2009;72(11):2005–2008. https://doi.org/10.1021/np900449r.
15 Chen H, Zhao Z, Cheng G, et al. Immunosuppressive nor-isopimarane diterpenes from cultures of the fungicolous fungus *Xylaria longipes* HFG1018. *J Nat Prod*. 2020;83(2):401–412. https://doi.org/10.1021/acs.jnatprod.9b00889.
16 Zhao Q, Tian J, Yue J, et al. Diterpenoids from isodon flavidus. *Phytochemistry*. 1998;48(6):1025–1029. https://doi.org/10.1016/S0031-9422(97)00608-0.
17 Wang J, Duan H, Wang Y, et al. *Ent*-strobane and *ent*-pimarane diterpenoids from *Siegesbeckia pubescens*. *J Nat Prod*. 2017;80(1):19–29. https://doi.org/10.1021/acs.jnatprod.6b00150.
18 Tan R, Hu Y, Liu Z, et al. New kaurane diterpenoids from *Aster tongolensis*. *J Nat Prod*. 1993;56(11):1917–1922. https://doi.org/10.1021/np50101a008.
19 Xiong J, Ma Y, Xu Y. Diterpenoids from *Siegesbeckia pubescens*. *Phytochemistry*. 1992;31(3):917–921. https://doi.org/10.1016/0031-9422(92)80039-H.
20 Yang Y, Chang F, Wu C, et al. New *ent*-kaurane diterpenoids with anti-platelet aggregation activity from *Annona squamosa*. *J Nat Prod*. 2002;65(10):1462–1467. https://doi.org/10.1021/np020191e.
21 Li Y, Ge JP, Ma K, et al. The combination of EGCG with warfarin reduces deep vein thrombosis in rabbits through modulating HIF-1α and VEGF *via* the PI3K/AKT and ERK1/2 signaling pathways. *Chin J Nat Med*. 2022;20(9):679–690. https://doi.org/10.1016/s1875-5364(22)60172-9.
22 Wang P, Huang Y, Ren J, et al. Large-leaf yellow tea attenuates high glucose-induced vascular endothelial cell injury by up-regulating autophagy and down-regulating oxidative stress. *Food Funct*. 2022;13(4):1890–1905. https://doi.org/10.1039/D1FO03405G.
23 Wang D, Wang Q, Yan G, et al. High glucose and interleukin 1*β*-induced apoptosis in human umbilical vein endothelial cells involves in down-regulation of monocarboxylate transporter 4. *Biochem Biophys Res Commun*. 2015;466(4):607–614. https://doi.org/10.1016/j.bbrc.2015.09.016.
24 Sorrentino FS, Matteini S, Bonifazzi C, et al. Diabetic retinopathy and endothelin system: microangiopathy versus endothelial dysfunction. *Eye (Lond)*. 2018;32(7):1157–1163. https://doi.org/10.1038/s41433-018-0032-4.
25 Wang M, Hsiao G, Al-Shabrawey M. Eicosanoids and oxidative stress in diabetic retinopathy. *Antioxidants (Basel)*. 2020;9(6):520. https://doi.org/10.3390/antiox9060520.
26 Kanwar M, Chan P, Kern T, et al. Oxidative damage in the retinal mitochondria of diabetic mice: possible protection by superoxide dismutase. *Invest Ophthalmol Vis Sci*. 2007;48(8):3805–3811. https://doi.org/10.1167/iovs.06-1280.
27 Kowluru R, Zhong Q, Santos J. Matrix metalloproteinases in diabetic retinopathy: potential role of MMP-9. *Expert Opin Investig Drugs*. 2012;21(6):797–805. https://doi.org/10.1517/13543784.2012.681043.
28 Reckamp KL, Gardner BK, Figlin RA, et al. Tumor response to combination celecoxib and erlotinib therapy in non-small cell lung cancer is associated with a low baseline matrix metalloproteinase-9 and a decline in serum-soluble E-cadherin. *J Thorac Oncol*. 2008;3(2):117–124. https://doi.org/10.1097/JTO.0b013e3181622bef.
29 Li C, Miao X, Li F, et al. Oxidative stress-related mechanisms and antioxidant therapy in diabetic retinopathy. *Oxid Med Cell Longev*. 2017;2017:9702820. https://doi.org/10.1155/2017/9702820.
30 Kowluru RA. Cross talks between oxidative stress, inflammation and epigenetics in diabetic retinopathy. *Cells*. 2023;12(2):300. https://doi.org/10.3390/cells12020300.
31 Liu Y, Wu H, Wang T, et al. Paeonol reduces microbial metabolite *α*-hydroxyisobutyric acid to alleviate the ROS/TXNIP/NLRP3 pathway-mediated endothelial inflammation in atherosclerosis mice. *Chin J Nat Med*. 2023;21(10):759–774. https://doi.org/10.1016/s1875-5364(23)60506-0.
32 Zheng L, Howell SJ, Hatala DA, et al. Salicylate-based anti-inflammatory drugs inhibit the early lesion of diabetic retinopathy. *Diabetes*. 2007;56(2):337–345. https://doi.org/10.2337/db06-0789.
33 Joussen AM, Poulaki V, Le ML, et al. A central role for inflammation in the pathogenesis of diabetic retinopathy. *FASEB J*. 2004;18(12):1450–1452. https://doi.org/10.1096/fj.03-1476fje.
34 Rübsam A, Parikh S, Fort PE. Role of inflammation in diabetic retinopathy. *Int J Mol Sci*. 2022;19(4):942. https://doi.org/10.3390/ijms19040942.
35 Shan P, Wang C, Chen H, et al. Inonotsutriol E from inonotus obliquus exhibits promising anti breast cancer activity *via* regulating the JAK2/STAT3 signaling pathway. *Bioorg Chem*. 2023;139:106741. https://doi.org/10.1016/j.bioorg.2023.106741.